Electronic Supplementary Material (ESI) for Journal of Materials Chemistry A.

Supporting Information

Sheet-dot-framework membrane towards efficient proton conduction and outstanding stability

Jianlong Lin[a,1], Jingchuan Dang[a,1], Guoli Zhou[a], Wenjia Wu[a,b,*], Yarong Liu[a], Yafang Zhang[a], Jingtao Wang[a,c,*]

[a]School of Chemical Engineering, Zhengzhou University, Zhengzhou 450001, P. R. China

[b]College of Chemistry, Zhengzhou University, Zhengzhou 450001, P. R. China

[c]Henan Institute of Advanced Technology, Zhengzhou University, 97 Wenhua Road Zhengzhou 450003, P.R. China

*To whom correspondence should be addressed: E-mail: wenjiawu@zzu.edu.cn (W.J. Wu); jingtaowang@zzu.edu.cn (J.T. Wang).

[1]These authors contributed equally to this work.

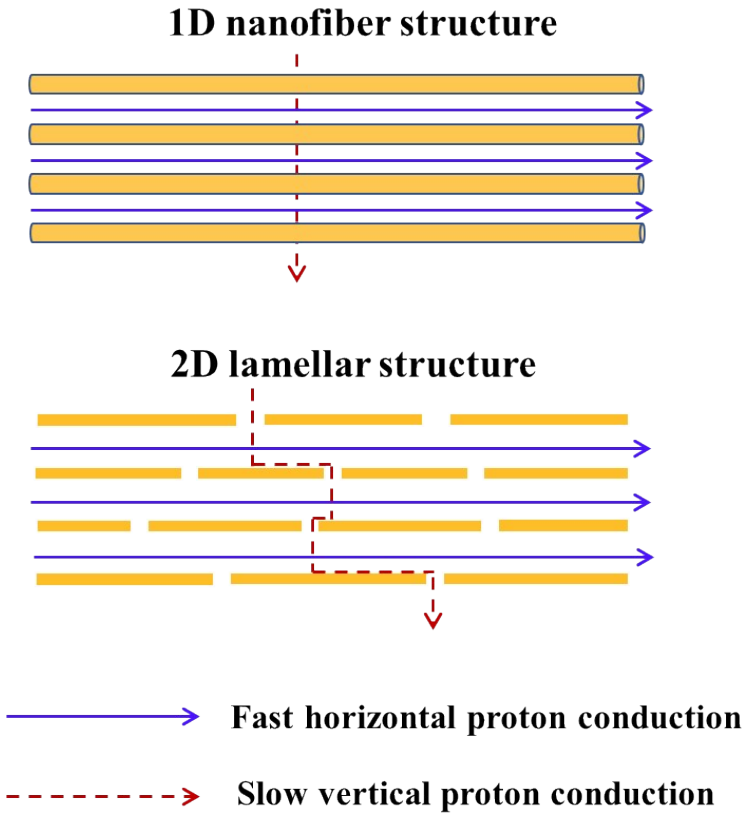

Fig. S1. Schematic of low-dimension (1D and 2D) structures for proton conduction.

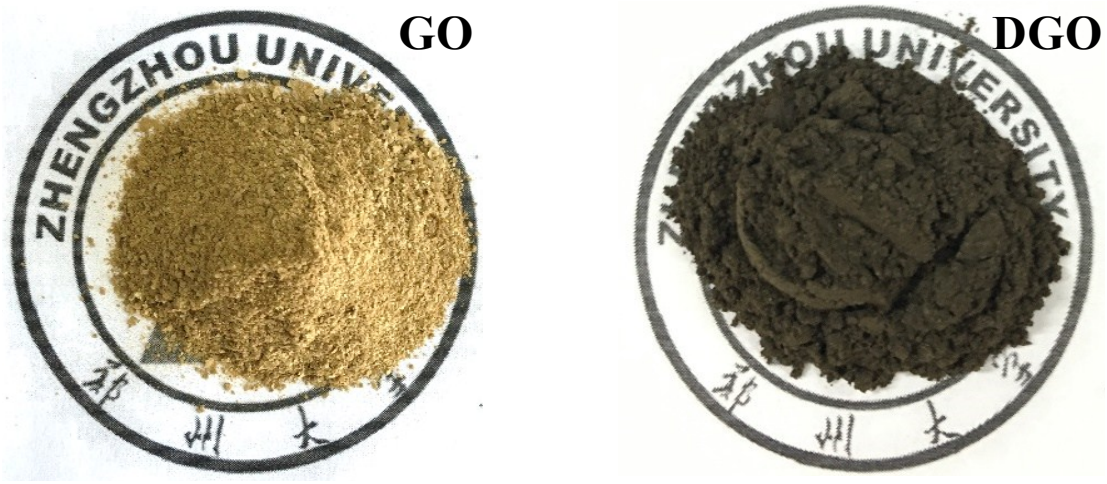

Fig. S2. Photos of GO and DGO powders.

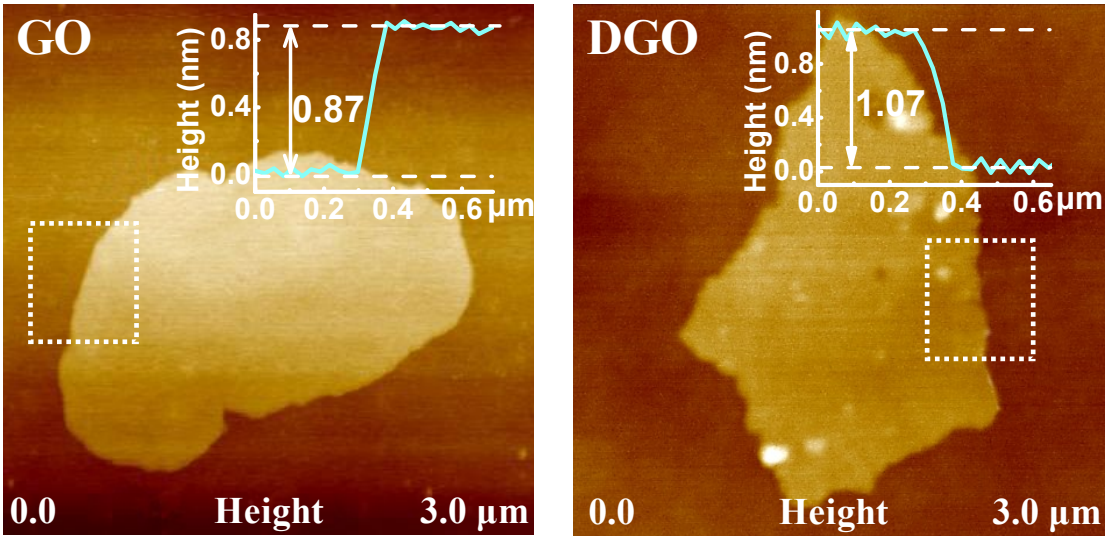

Fig. S3. AFM images and the corresponding height profiles of GO and DGO nanosheets.

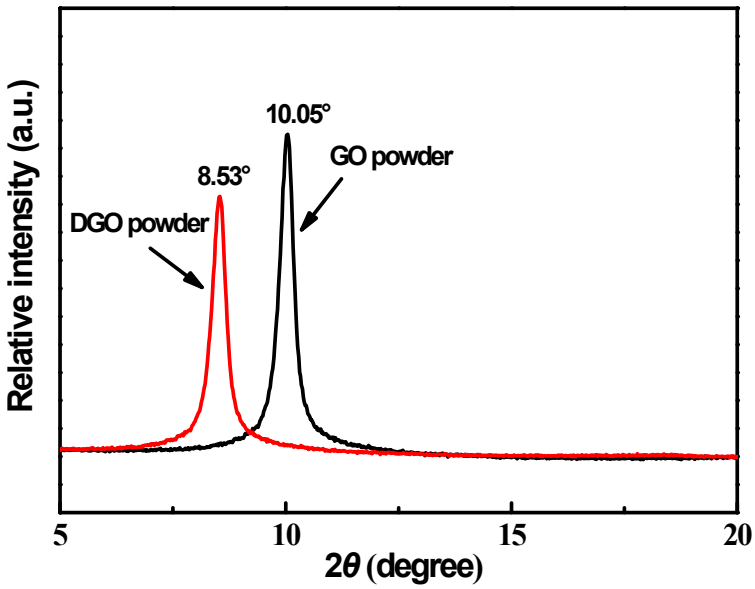

Fig. S4. XRD patterns of GO and DGO nanosheets.

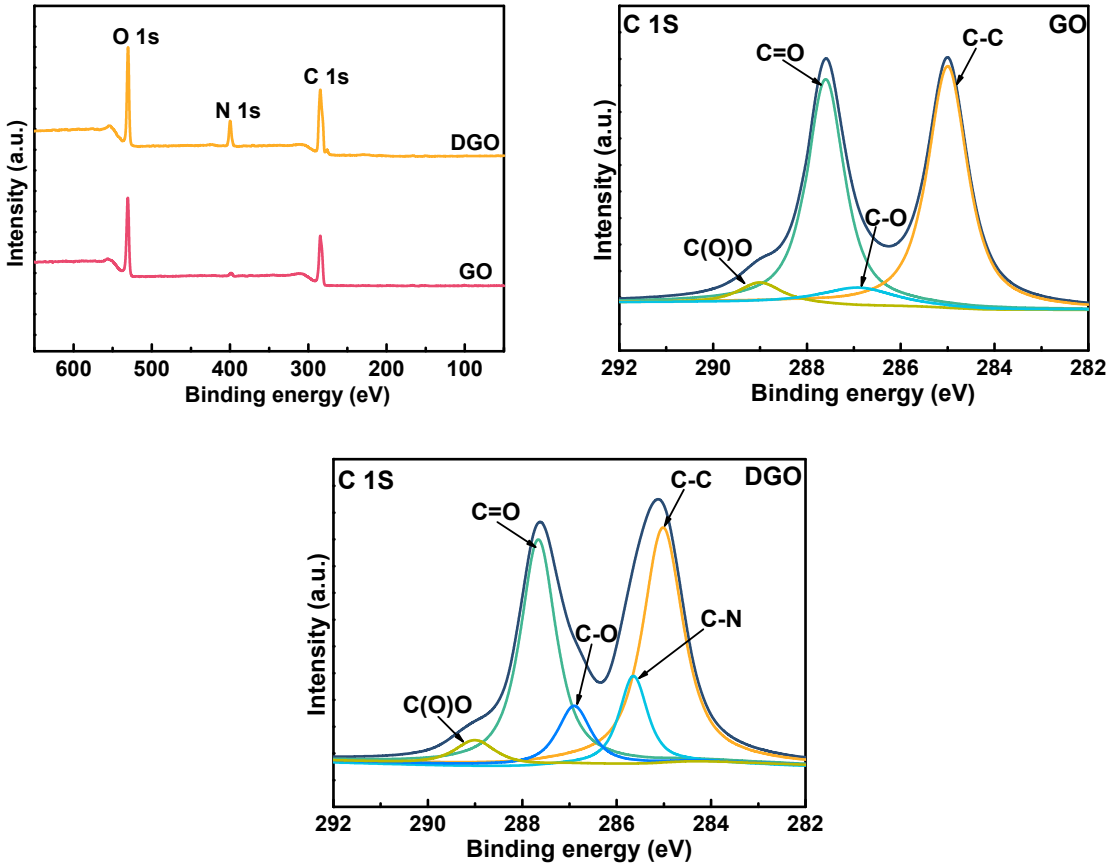

Fig. S5. XPS spectra of GO and DGO nanosheets.

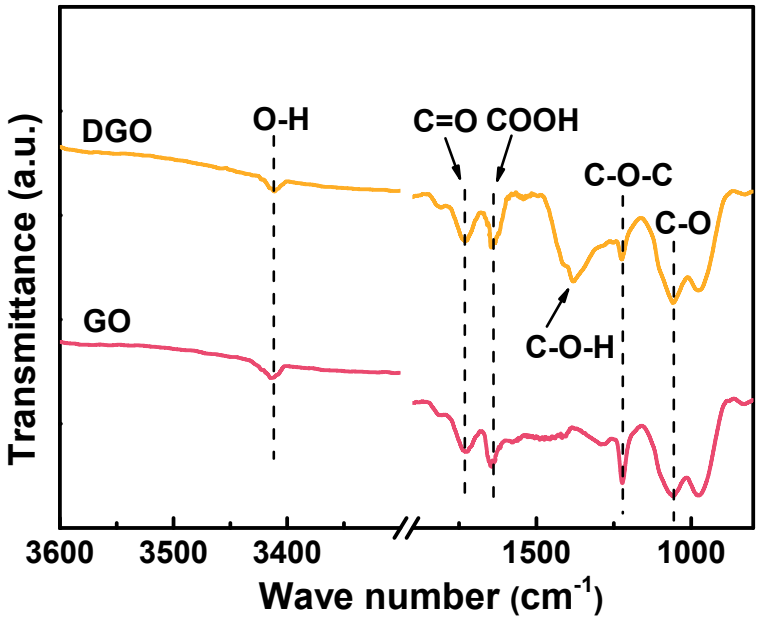

Fig. S6. FTIR spectra of GO and DGO nanosheets.

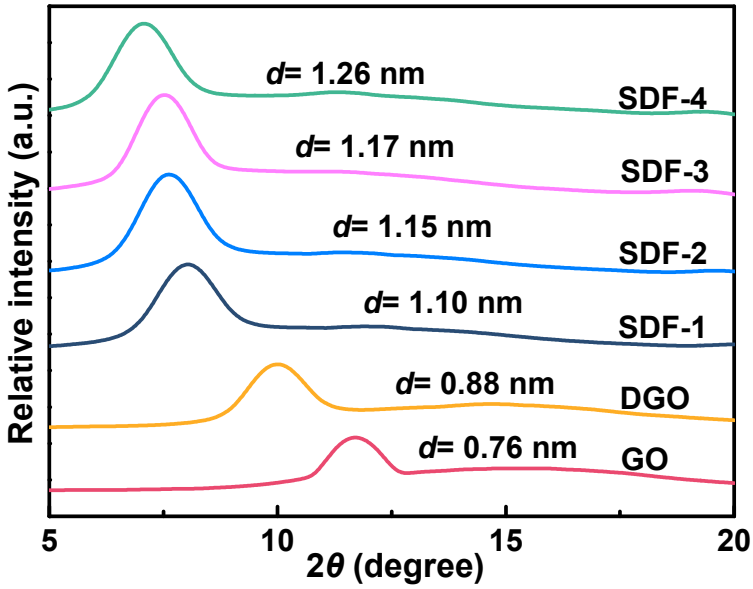

Fig. S7. XRD patterns of the membranes.

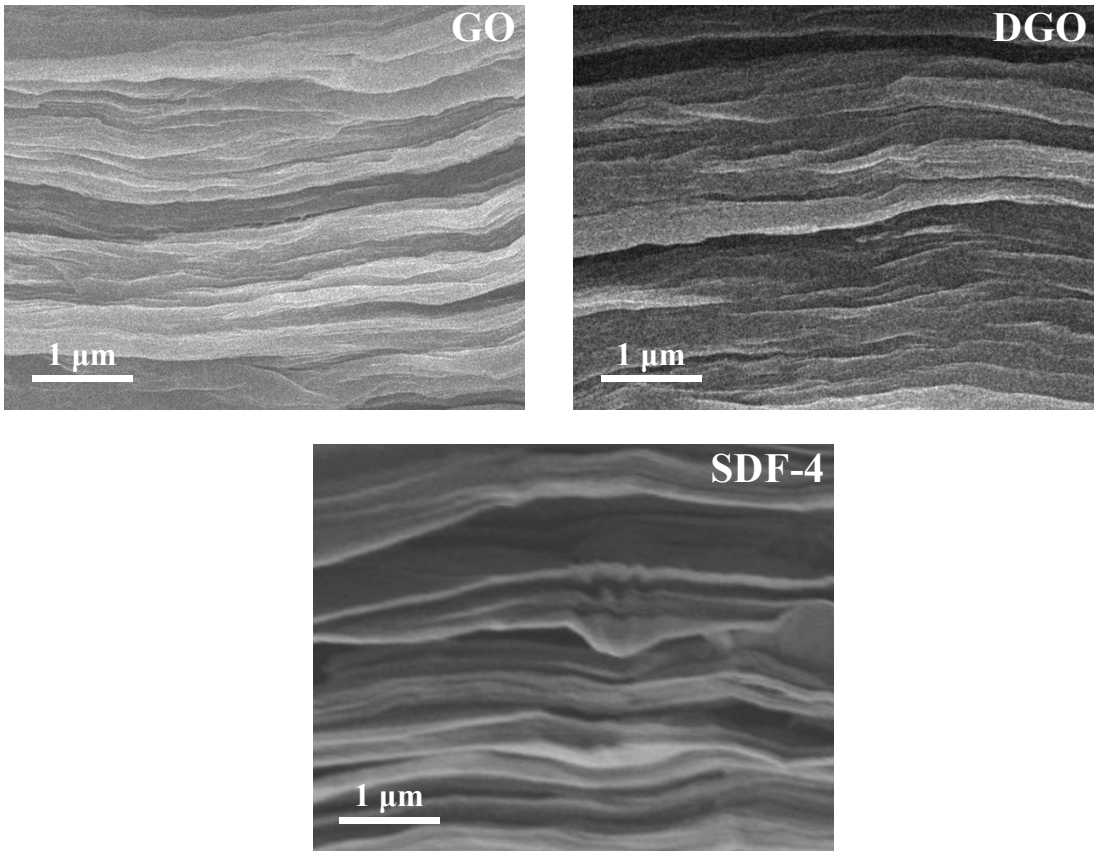

Fig. S8. Cross-sectional SEM images of GO, DGO, and SDF-4 membranes.

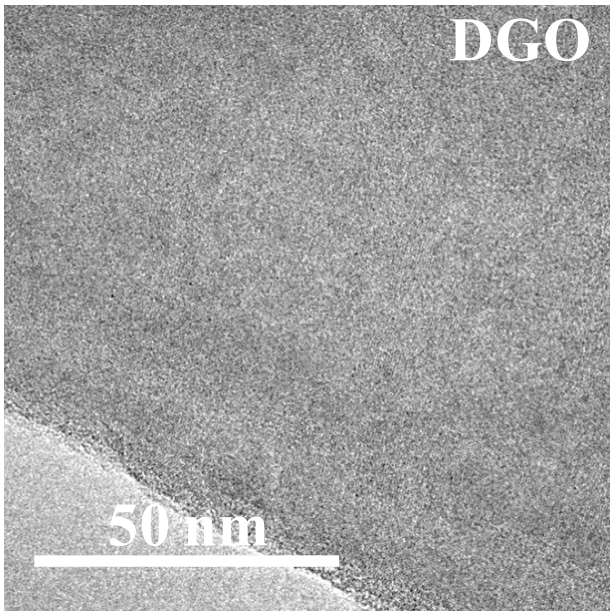

Fig. S9. TEM image of DGO nanosheet.

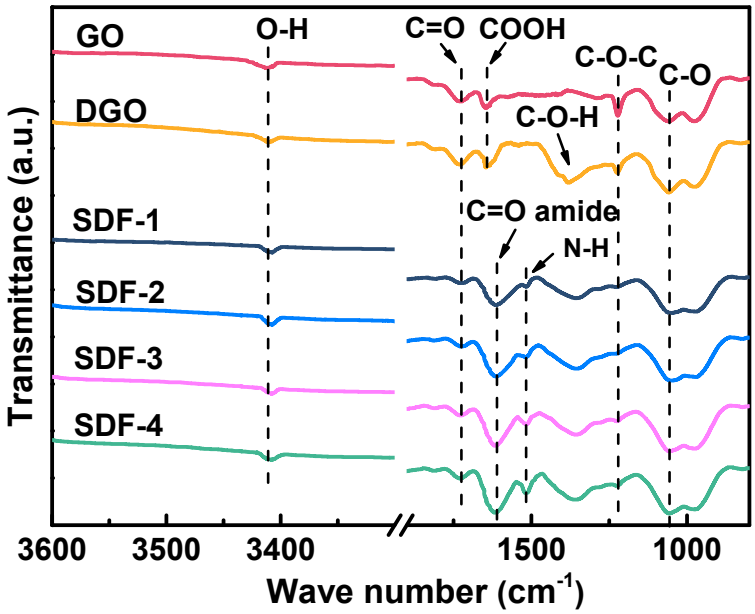

Fig. S10. FTIR spectra of the membranes.

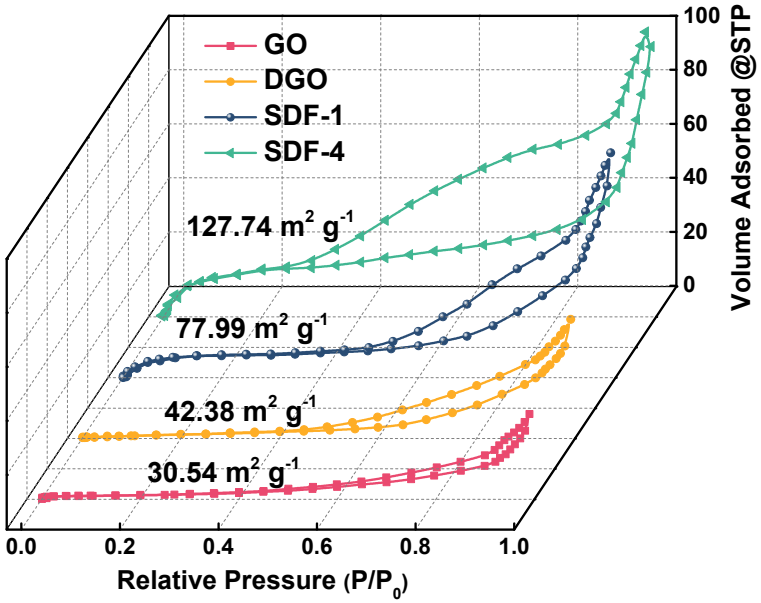

Fig. S11. Nitrogen adsorption/desorption isotherms and surface area of the membranes.

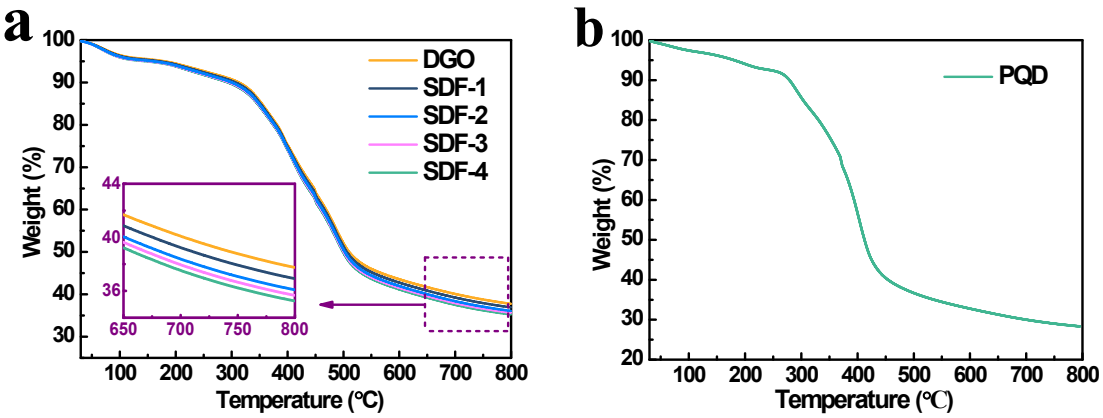

Fig. S12. TGA curves of a) membranes and b) PQD.

Fig. S13. Water contact angle of the membranes.

Fig. S14. Photos of the stability of GO, SDF-1, SDF-2, and SDF-3 membranes under ultrasonic treatment for 4 h.

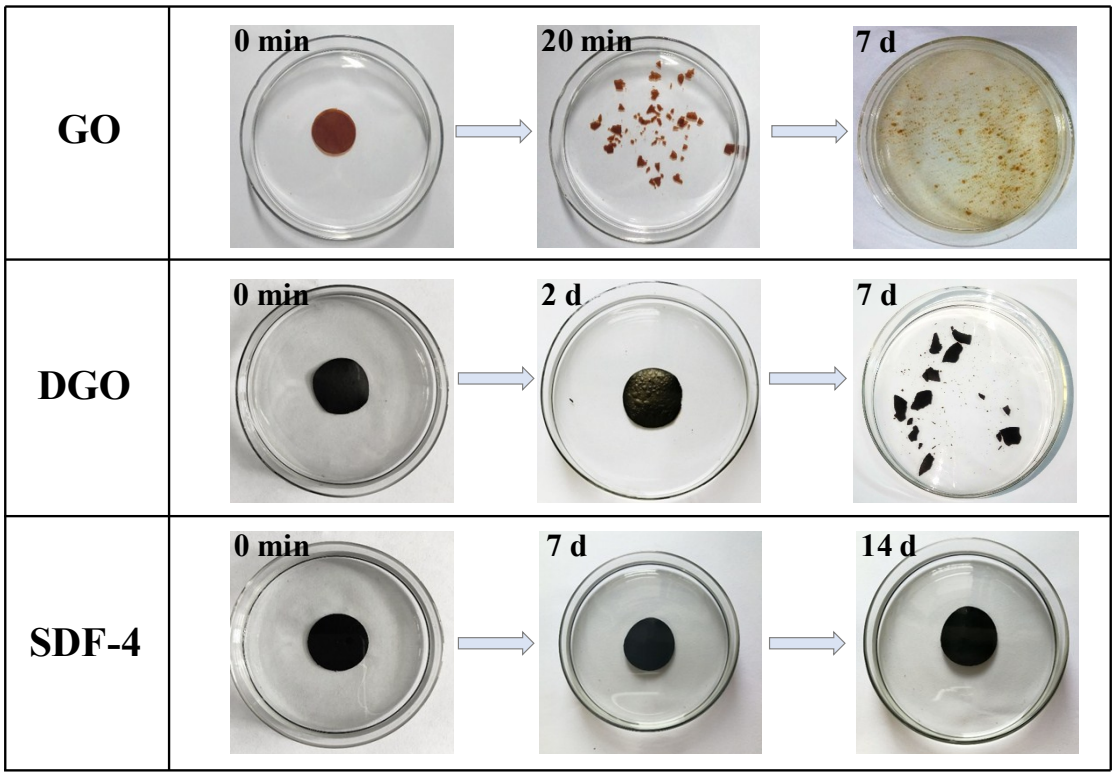

Fig. S15. Photos of the stability of GO, DGO, and SDF-4 membranes soaking in water at pH=7 for different time.

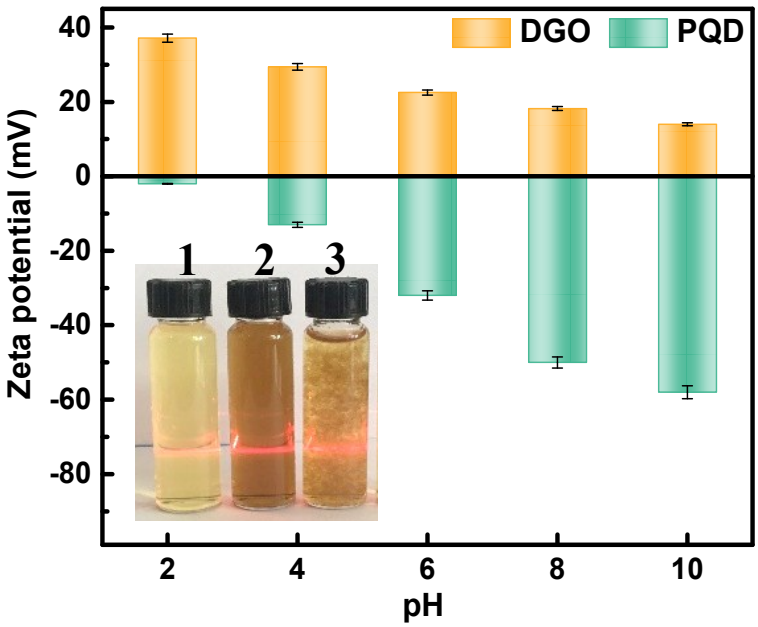

Fig. S16. Zeta potential of the DGO aqueous solution (1 g L^{-1}) and the PQD aqueous solution (1 g L^{-1}) with pH of 2-10 (insets are the photographs of PQD solution (1), DGO solution (2), and the mixed solution of PQD and DGO (3)).

Fig. S17. Photo of the stability of DGO/PQD membrane soaking in water for 2 d.

Fig. S18. Photos of the stability of SDF-4 membrane in different pH aqueous solutions for 14 d.

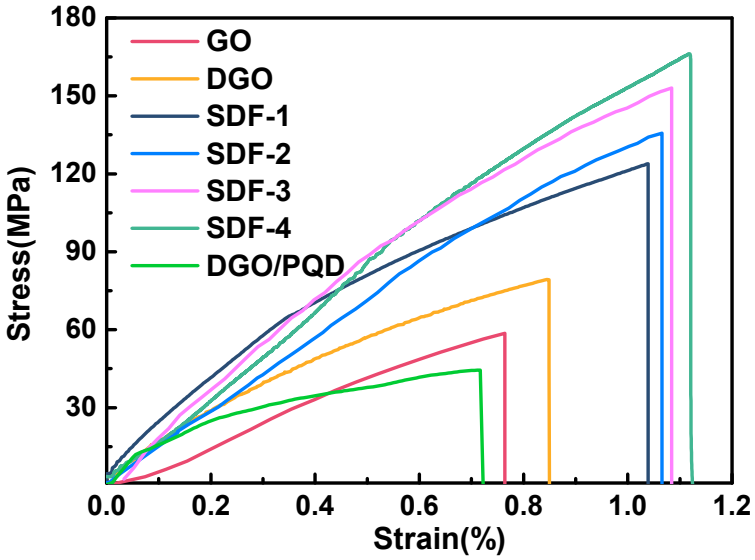

Fig. S19. Stress-strain curves of the membranes.

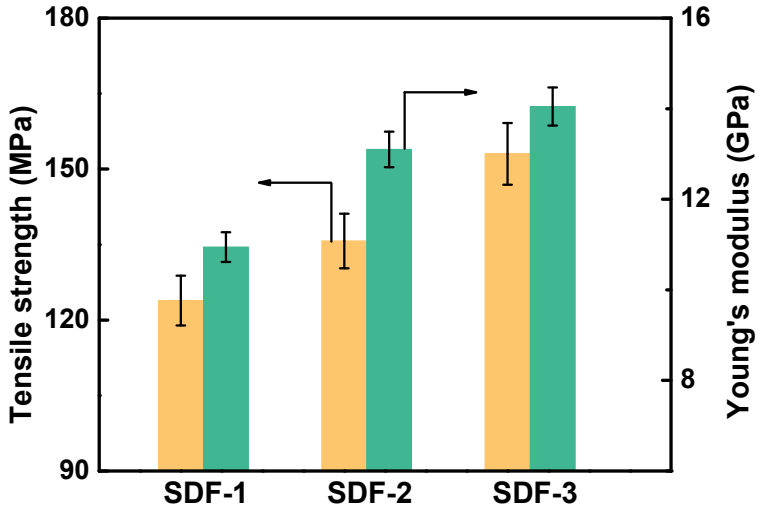

Fig. S20. Tensile strength and elastic modulus of SDF-1, SDF-2, and SDF-3 membranes.

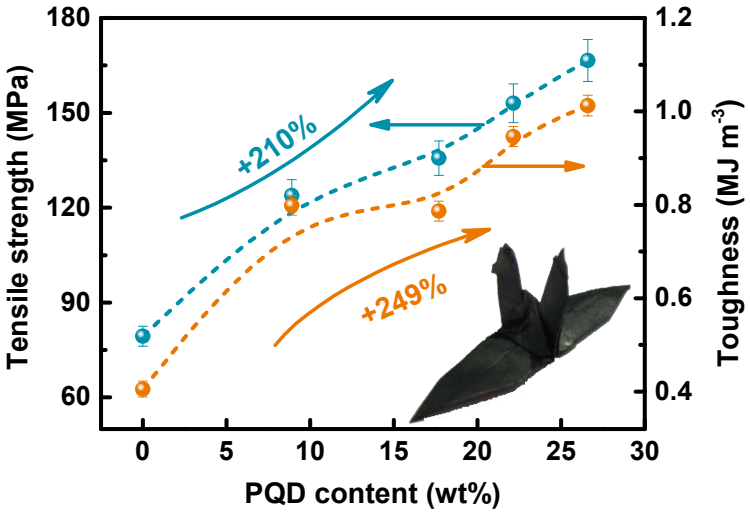

Fig. S21. The mechanical properties of the membranes (inset is a paper cranes folded with SDF-4 membrane).

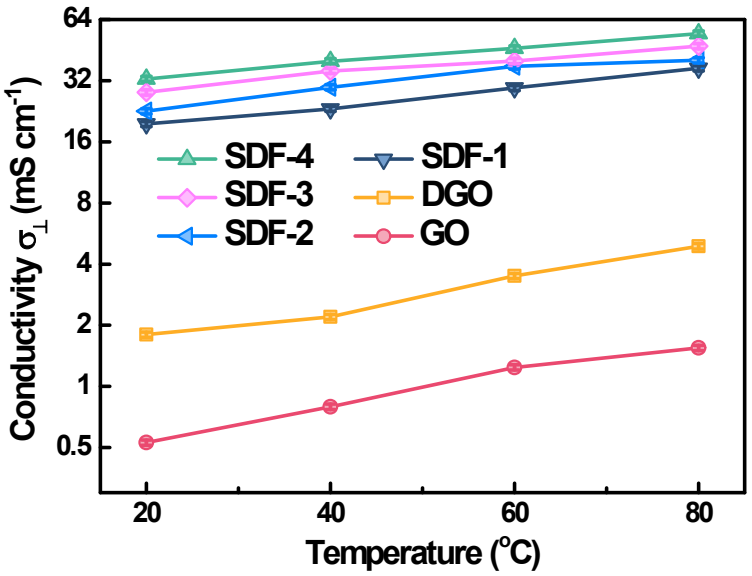

Fig. S22. Temperature-dependent vertical proton conductivities of the membranes under 100% RH.

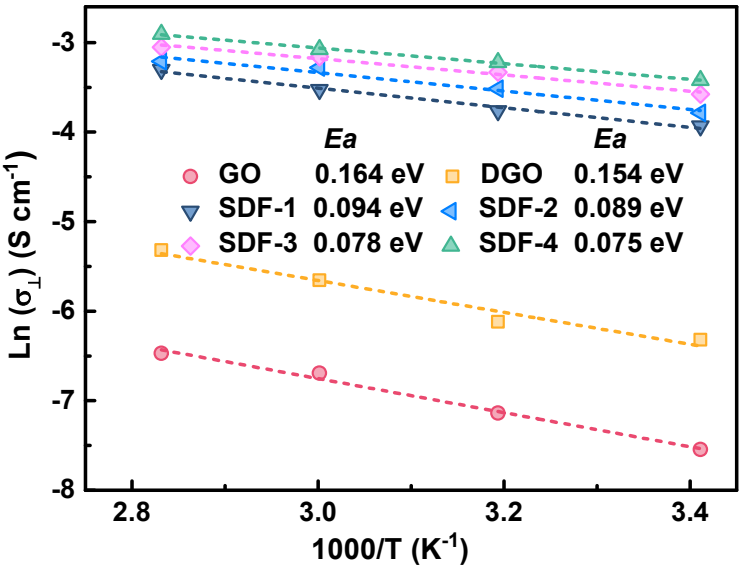

Fig. S23. Arrhenius plots of vertical conductivity under 100% RH and the related activation energy values.

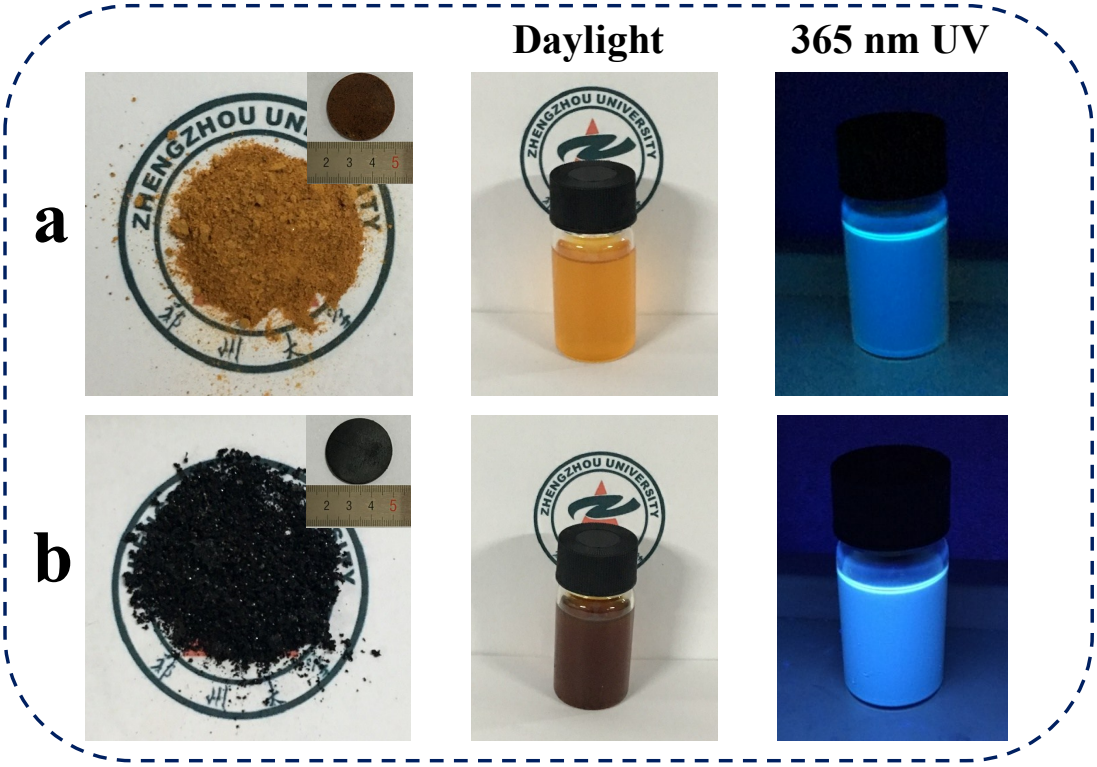

Fig. S24. Powders, tableting, and fluorescence effect of solution under daylight and 365 nm UV of a) PQD and b) C-PQD.

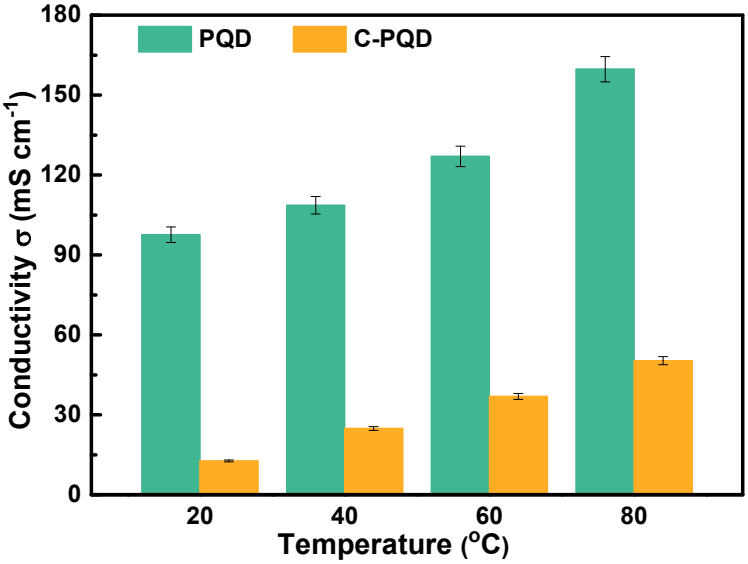

Fig. S25. Temperature-dependent proton conductivities of PQD and C-PQD under 100% RH.

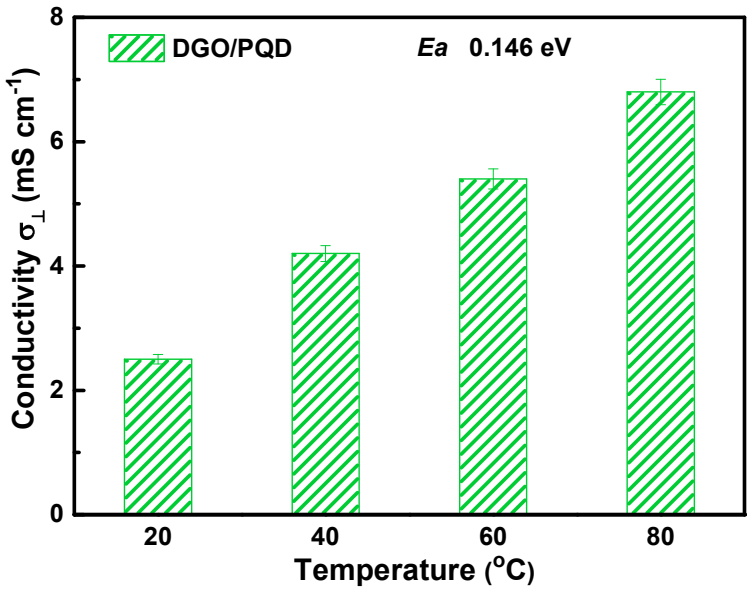

Fig. S26. Temperature-dependent proton conductivities of DGO/PQD membrane under 100% RH.

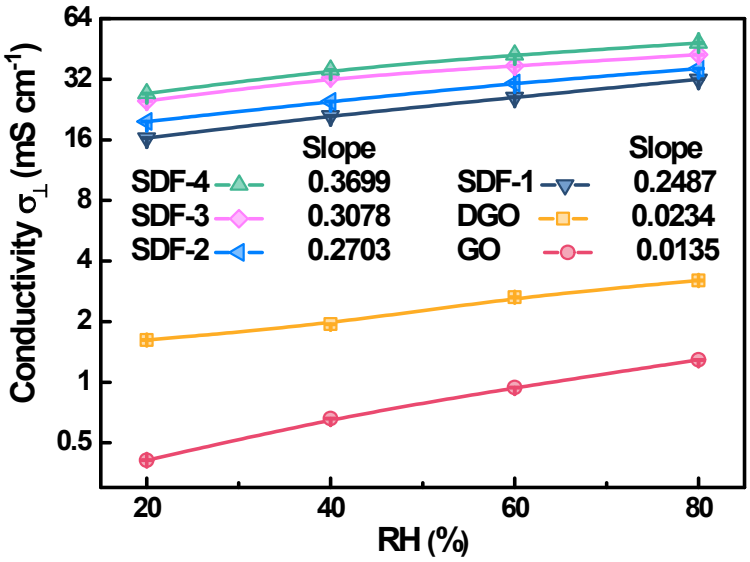

Fig. S27. Humidity-dependent vertical proton conductivities of the membranes at 80 °C.

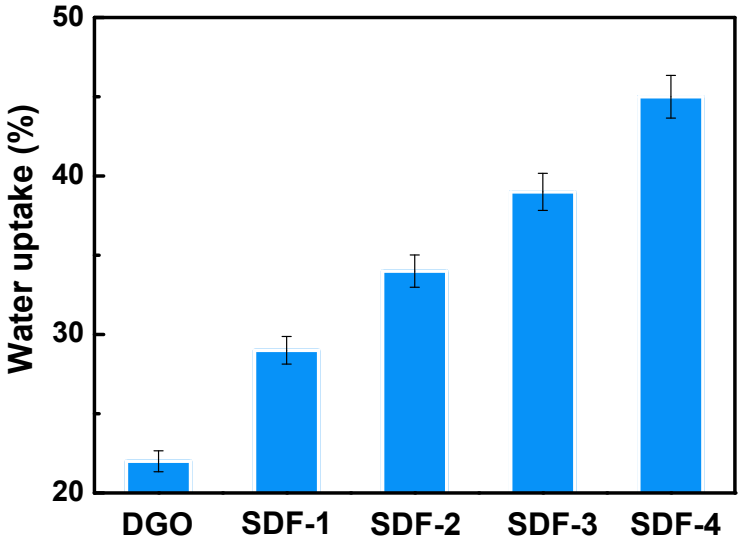

Fig. S28. Water uptake of the membranes at 30 °C.

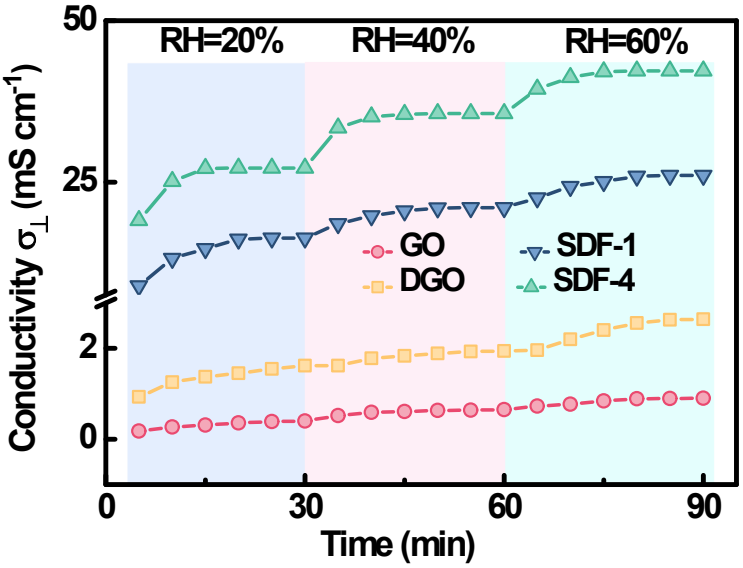

Fig. S29. Time-dependent vertical proton conductivities of the membranes at 80 °C.

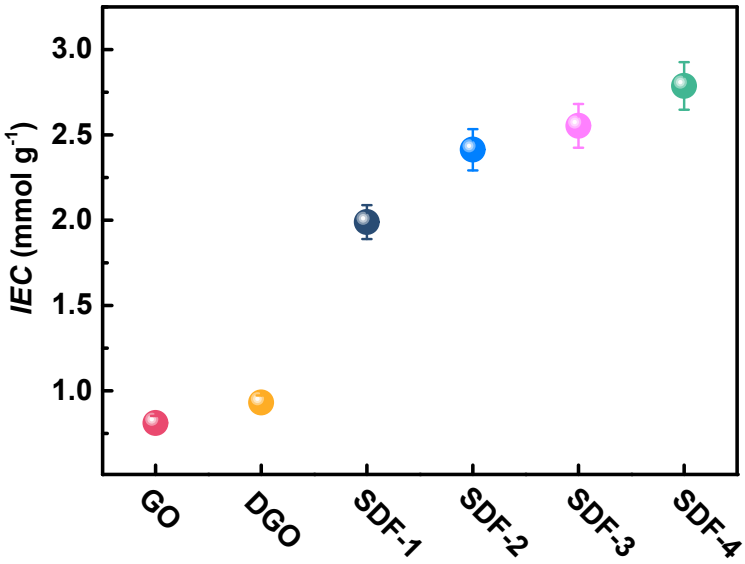

Fig. S30. *IEC* values of the membranes.

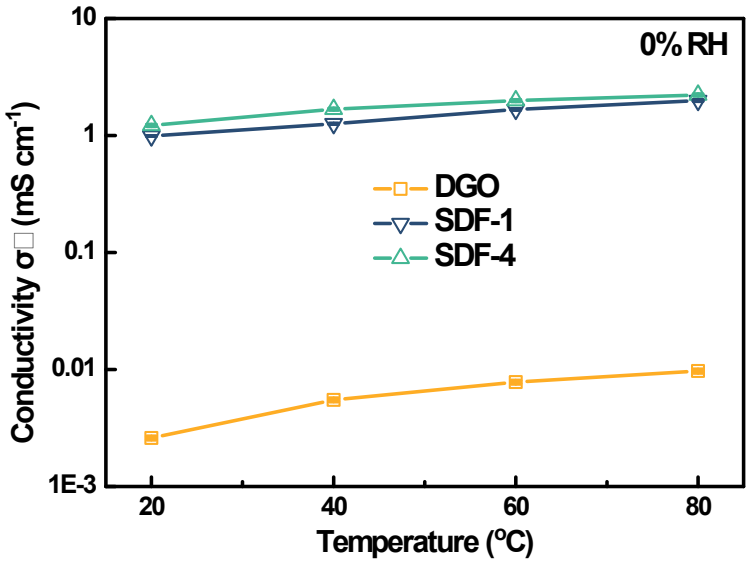

Fig. S31. Temperature-dependent vertical conductivities of DGO, SDF-1, and SDF-4 membranes under anhydrous conditions.

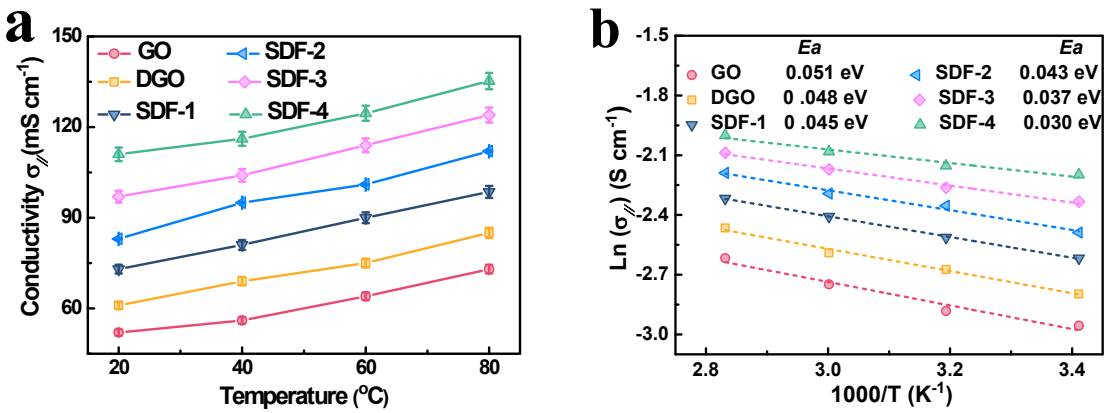

Fig. S32. a) Temperature-dependent horizontal conductivities of the membranes under 100% RH. b) Arrhenius plots of horizontal conductivities under 100% RH and the related activation energy values.

Table S1. The recipe and calculated PQD content in SDF membranes, and the average thickness of as-prepared membranes

Sample	Solution concentration ($mol \cdot L^{-1}$)		Char yield (%)	PQD content (wt %)	Thickness (μm)
	DETA	CA			
GO	-	-	-	-	15±2
DGO	-	-	37.76	-	16±1
SDF-1	0.005	0.005	36.92	8.9	18±3
SDF-2	0.01	0.01	36.09	17.7	17±2
SDF-3	0.025	0.025	35.67	22.1	18±2
SDF-4	0.016	0.016	35.23	26.6	20±3

Table S2. Comparison of mechanical properties of SDF membranes with other GO-based membranes

Membrane	Tensile strength (MPa)	Elongation at break (%)	Young's modulus (GPa)	Toughness (MJ m^{-3})	Ref.
GO paper	58.61	0.76	8.21	0.23	-
GO-MMT	112.3	1.45	13.74	0.988	[1]
GO-Borate	~160	~0.24	-	-	[2]
GO-GA	~101	~0.4	~30.4	~0.3	[3]
GO-GA-H_2O	~93	~1.3	~14.4	~0.8	
GO-Ca^{2+}	134.8	0.68	28.1	-	[4]
GO-Mg^{2+}	124.9	0.47	30.5	-	
GO-PAA	91.9	0.32	-	0.18	[5]
GO-PVA	71	0.27	27.6	0.1	[6]
GO-PMMA	148.3	3.17	7.5	2.35	
GO-PCDO	~106.6	~4.5	-	~2.52	[7]
GO/SGQD-PA-100	~55	-	-	-	[8]
PGO	29.1	16.4	0.73	-	[9]
PGO-PEI	185.3	0.238	86.34	-	[10]
rGO paper	150	0.83	-	0.62	[11]
rGO-PCDO	~129.6	~6.9	-	~3.91	[7]
rGO-PVA	188.9	2.67	10.4	-	[12]
rGO-SF	153	2.8	13	2.6	[13]
rGO-PAA	~309.57	~8.4	~4.57	~8.88	[14]
DGO	79.35	0.85	8.89	0.41	
SDF-1	123.88	1.04	10.94	0.8	This work
SDF-4	166.56	1.12	15.22	1.12	

- Not reported

Table S3. Comparison of proton conductivities of SDF membranes with other GO-based membranes

Fabrication method	Samples	Testing conditions	Horizontal proton conductivity ($mS \cdot cm^{-1}$)	Vertical proton conductivity ($mS \cdot cm^{-1}$)	Anisotropy coefficient	Ref.
Tabletting	GO nanosheet	85 °C, 100% RH,	150	-	-	[15]
	GO pellet	60 °C, 0% RH,	-	~0.08	-	[16]
	GO/HBS pellet	60 °C, 0% RH,	-	~0.36	-	
	GO/ABZ pellet	60 °C, 0% RH,	-	~0.59	-	
Solution casting method	SP-SGO membrane	150 °C, 0% RH	-	21.9	-	[17]
	Nafion/PGO membrane	80 °C, 40% RH	-	44.1	-	[18]
	CS-PGO-2.5 membrane	45 °C,100% RH	-	31	-	[19]
	SPEEK/DGO-10 membrane	30 °C,100% RH	-	26.4	-	[20]
	Nafion@3D sGO-3.6 membrane	80 °C, 98% RH	330	290	1.1	[21]
	SPEEK@3D sGO-2.4 membrane	80 °C, 98% RH	300	270	1.1	
	Fe_3O_4-sGO/PVA membrane	25 °C, 100% RH	-	64	-	[22]
	AQSA-GO membrane	25 °C, 100% RH	30	6	5.0	[23]
Spray painting method	GO membrane	70 °C, 100% RH	49.8	0.5	99.6	[24]
Langmuir-Blodgett method	Single-layer GO membrane	25 °C, 90% RH	0.2	-	-	[25]
Drop-cast method	Multilayer GO membrane	25 °C, 60% RH	0.4	-	-	
Vacuum filtration	GO-MPS membrane	30 °C, 100% RH	2.09	-	-	[9]
	PGO membrane	80 °C, 51% RH	32	-	-	
	N-srGOM membrane	80 °C, 95% RH	580	-	-	[26]
	OGO membrane	45 °C, 100% RH	230	-	-	[27]
	$\{H_6Bi_{12}O_{16}\}$/GO membrane	80 °C, in aqueous solution	564	-	-	[28]
	SGO membrane	30 °C, 100% RH	40	12	3.3	[29]
	GO/SGQD-PA-100	30 °C, 100% RH	159	~4.2	~37.9	[8]
	GO/MMT/SPVA-30 membrane	30 °C, 100% RH	92.1	-	-	[1]
	DGO membrane	80 °C, 100% RH	85	4.9	17.3	This work
	SDF-1	80 °C, 100% RH	98.6	36.8	2.7	
	SDF-4	80 °C, 100% RH	135.3	54.6	2.5	

- Not reported

Table S4. Comparison of proton conductivity and mechanical property of SDF membranes with other GO-based membranes

Membranes		Testing conditions	Proton conductivity ($mS \cdot cm^{-1}$)	Tensile strength (MPa)	Ref.
GO laminate	Spray-painted GO	70 °C, 100% RH	0.5[a]	54.5	[24]
	GO	70 °C, 100% RH	0.55[a]	~56	[30]
	DGO	80 °C, 100% RH	4.9[a]	79.35	-
	PGO	80 °C, 51% RH	32[b]	29.1	[9]
	SGO	30 °C, 100% RH	12[a]	~20	[29]
	GO/SGQD-PA-100	30 °C, 100% RH	~4.2[a]	~55	[8]
Polymer-GO composite	SP-SGO	150 °C, 0% RH	21.9[a]	36.6	[17]
	CS-PGO	45 °C,100% RH	31[a]	51.5	[19]
	SPEEK-DGO	30 °C,100% RH	26.4[a]	57.5	[20]
	Fe_3O_4-sGO/PVA	25 °C, 100% RH	64[a]	~76.2	[22]
	SPEEK-ASPGO	80 °C, 100% RH	~110[b]	~41	[31]
	SP/I-P-@SiGO	120 °C, 0% RH	4.3[a]	~40	[32]
	CS/S4GO	120 °C, 0% RH	10.9[a]	85.3	[33]
Commercial Nafion	Nafion 117	30 °C, 100% RH	76.8[a]	~25	[9]
Sheet-dot framework	SDF-1	80 °C, 100% RH	36.8[a]	123.88	This work
	SDF-4	80 °C, 100% RH	54.6[a]	166.56	

[a] vertical proton conductivity; [b] horizontal proton conductivity

Supplementary References

1 G. He, M. Xu, J. Zhao, S. Jiang, S. Wang, Z. Li, X. He, T. Huang, M. Cao, H. Wu, M. D. Guiver and Z. Jiang, *Adv. Mater.*, 2017, **29**, 1605898.

2 Z. An, O. C. Compton, K. W. Putz, L. C. Brinson and S. T. Nguyen, *Adv. Mater.*, 2011, **23**, 3842–3846.

3 Y. Gao, L. Q. Liu, S. Z. Zu, K. Peng, D. Zhou, B. H. Han and Z. Zhang, *ACS Nano*, 2011, **5**, 2134–2141.

4 S. Park, K. S. Lee, G. Bozoklu, W. Cai, S. T. Nguyen and R. S. Ruoff, *ACS Nano*, 2008, **2**, 572–578.

5 S. Park, D. A. Dikin, S. T. Nguyen and R. S. Ruoff, *J. Phys. Chem. C*, 2009, **113**, 15801–15804.

6 K. W. Putz, O. C. Compton, M. J. Palmeri, S. T. Nguyen and L. C. Brinson, *Adv. Funct. Mater.*, 2010, **20**, 3322–3329.

7 Q. Cheng, M. Wu, M. Li, L. Jiang and Z. Tang, *Angew. Chem., Int. Ed.*, 2013, **52**, 3750–3755.

8 B. Shi, H. Wu, J. Shen, L. Cao, X. He, Y. Ma, Y. Li, J. Li, M. Xu, X. Mao, M. Qiu, H. Geng, P. Yang and Z. Jiang, *ACS Nano*, 2019, **13**, 10366–10375.

9 G. He, C. Chang, M. Xu, S. Hu, L. Li, J. Zhao, Z. Li, Z. Li, Y. Yin, M. Gang, H. Wu, X. Yang, M. D. Guiver and Z. Jiang, *Adv. Funct. Mater.*, 2015, **25**, 7502–7511.

10 Y. Tian, Y. Cao, Y. Wang, W. Yang and J. Feng, *Adv. Mater.*, 2013, **25**, 2980–2983.

11 H. Chen, M. B. Müller, K. J. Gilmore, G. G. Wallace and D. Li, *Adv. Mater.*, 2008, **20**, 3557–3561.

12 Y. Q. Li, T. Yu, T. Y. Yang, L. X. Zheng and K. Liao, *Adv. Mater.*, 2012, **24**, 3426–3431.

13 K. Hu, L. S. Tolentino, D. D. Kulkarni, C. Ye, S. Kumar and V. V. Tsukruk, *Angew. Chem., Int. Ed.*, 2013, **52**, 13784–13788.

14 S. Wan, H. Hu, J. Peng, Y. Li, Y. Fan, L. Jiang and Q. Cheng, *Nanoscale*, 2016, **8**, 5649–5656.

15 M. R. Karim, K. Hatakeyama, T. Matsui, H. Takehira, T. Taniguchi, M. Koinuma, Y. Matsumoto, T. Akutagawa, T. Nakamura, S. I. Noro, T. Yamada, H. Kitagawa and S. Hayami, *J. Am. Chem. Soc.*, 2013, **135**, 8097–8100.

16 J. Wang, L. Zhao, D. Wei, W. Wu, J. Zhang and X. Cheng, *Ind. Eng. Chem. Res.*, 2016, **55**, 11931–11942.

17 W. Wu, Y. Li, P. Chen, J. Liu, J. Wang and H. Zhang, *ACS Appl. Mater. Interfaces*, 2016, **8**, 588–599.

18 B. Zhang, Y. Cao, S. Jiang, Z. Li, G. He and H. Wu, *J. Membr. Sci.*, 2016, **518**, 243–253.

19 H. Bai, Y. Li, H. Zhang, H. Chen, W. Wu, J. Wang and J. Liu, *J. Membr. Sci.*, 2015, **495**, 48–60.

20 Y. He, J. Wang, H. Zhang, T. Zhang, B. Zhang, S. Cao and J. Liu, *J. Mater. Chem. A*, 2014, **2**, 9548–9558.

21 L. Cao, H. Wu, P. Yang, X. He, J. Li, Y. Li, M. Xu, M. Qiu and Z. Jiang, *Adv. Funct. Mater.*, 2018, **28**, 1804944.

22 H. Beydaghi and M. Javanbakht, *Ind. Eng. Chem. Res.*, 2015, **54**, 7028–7037.

23 M. Gautam, M. C. Devendrachari, R. Thimmappa, A. R. Kottaichamy, S. P. Shafi, P. Gaikwad, H. M. N. Kotresh and M. O. Thotiyl, *Phys. Chem. Chem. Phys.*, 2017, **19**, 7751–7759.

24 T. Bayer, R. Selyanchyn, S. Fujikawa, K. Sasaki and S. M. Lyth, *J. Membr. Sci.*, 2017, **541**, 347–357.

25 K. Hatakeyama, M. R. Karim, C. Ogata, H. Tateishi, A. Funatsu, T. Taniguchi, M. Koinuma, S. Hayami and Y. Matsumoto, *Angew. Chem., Int. Ed.*, 2014, **126**, 7117–7120.

26 W. Jia, B. Tang and P. Wu, *ACS Appl. Mater. Interfaces*, 2017, **9**, 22620–22627.

27 W. Gao, G. Wu, M. T. Janicke, D. A. Cullen, R. Mukundan, J. K. Baldwin, E. L. Brosha, C. Galande, P. M. Ajayan, K. L. More, A. M. Dattelbaum and P. Zelenay, *Angew. Chem., Int. Ed.*, 2014, **53**, 3588–3593.

28 B. Liu, D. Cheng, H. Zhu, J. Du, K. Li, H. Y. Zang, H. Tan, Y. Wang, W. Xing and Y. Li, *Chem. Sci.*, 2019, **10**, 556–563.

29 Ravikumar and K. Scott, *Chem. Commun.*, 2012, **48**, 5584–5586.

30 T. Bayer, S. R. Bishop, M. Nishihara, K. Sasaki and S. M. Lyth, *J. Power Sources*, 2014, **272**, 239–247.

31 G. Rambabu and S. D. Bhat, *J. Membr. Sci.*, 2018, **551**, 1–11.

32 J. Wang, H. Bai, J. Zhang, L. Zhao, P. Chen, Y. Li and J. Liu, *J. Membr. Sci.*, 2017, **531**, 47–58.

33 Y. Liu, J. Wang, H. Zhang, C. Ma, J. Liu, S. Cao and X. Zhang, *J. Power Sources*, 2014, **269**, 898–911.